Electronic Supplementary Material (ESI) for Journal of Materials Chemistry A.

Electronic Supplementary Information

Porphyrinic porous organic frameworks: preparation and post-synthetic modification via demetallation-remetallation

Qipu Lin,[a] Jingzhi Lu,[a] Zhaodi Yang,[a, b] Xiaocheng Zeng,[a] and Jian Zhang[a]*

[a] Department of Chemistry, University of Nebraska-Lincoln, Lincoln, Nebraska 68588, USA

[b] College of Chemical and Environmental Engineering, Harbin University of Science and Technology, Harbin 150040, China

* *E-mail: jzhang3@unl.edu*

Table of Contents

A. Gas sorption study

N_2, H_2, and CO_2 gas sorption experiments were carried out on a Micromeritics ASAP 2020 surface area and pore size analyzer. Prior to the measurement, the as-synthesized samples were rigorously washed by Soxhlet extraction. After dried in the vacuum oven for overnight, the samples were further activated using the "degas" function of the surface area analyzer for 12 hours at 200 ^oC. Liquid N_2, liquid Ar, acetone-dry ice, ice water, and water were used as the temperature controlling media for 77, 87, 195, 273, and 298 K, respectively. Pore size distribution was calculated from the N_2 sorption isotherms based on the NLDFT model in the Micromeritics ASAP 2020 software package.

The isosteric heats of adsorption (Q_{st}) were calculated using a virial type thermal equation given below:

$$\ln(P) = \ln(n) + \frac{1}{T}\sum_{i=0}^{x} a_i n^i + \sum_{i=0}^{y} b_i n^i$$

where the pressure (P) is expressed in mmHg, the amount absorbed (n) is expressed in mmol/g, and the temperature (T) is expressed in K. The virial coefficients a_i and b_i were fit by increasing the respective number of each (x and y) until a sufficient goodness of fit was reached. The values of the virial coefficients a_0 to a_x were then used to calculate the isosteric heat of adsorption (Q_{st}) based on the equation given below:

$$Q_{st} = -R\sum_{i=0}^{x} a_i n^i$$

B. Synthesis of monomers

5,10,15,20-Tetrakis(4-trimethylsilyl-ethynyl)porphyrin-zinc (II) (**P1-TMS-Zn**): Under argon, borontrifluoride etherate ($BF_3{\cdot}Et_2O$, 0.32 mL, 2.6 mmol) was added to a solution of pyrrole (3.5 mL, 50 mmol) and trimethylsilylpropynal (7.4 mL, 50 mmol) in CH_2Cl_2 (750 mL) and the solution was stirred at -78 °C for 3 h. The mixture was allowed to warm to room temperature. 2,3-dichloro-5,6-dicyano-1,4-benzoquinone (DDQ, 11.5g, 50 mmol) was added and the stirring continued for 5 min. The resulted solution was filtered through silica. The solvent was removed under reduced pressure and the residue was dissolved in CH_2Cl_2 and filtered through a short plug of silica again before further purification by flash chromatography (SiO_2/CH_2Cl_2/*n*-hexane) and recrystallization from dichloromethane/methanol. The resulting compound (1.2 g, 1.75 mmol) and $Zn(OAc)_2{\cdot}2H_2O$ (2.2 g, 10 mmol, dissolved in 60 mL MeOH) in $CHCl_3$ (250 mL) was heated at reflux for 6 h. Water was added to the mixture, which ws evaporated under reduced pressure to remove chloroform and methanol, and the residue was filtered to produce a purple powder. ^{1}H NMR (400 MHz, $CDCl_3$): δ = 0.646 (s, 36H, $SiMe_3$), 9.560 (s, 8H, β-pyrrole) ppm. MS (TOF MS ES+): calcd. for $C_{40}H_{44}N_4Si_4Zn$ [+] 756.1935; found *m*/*z* = 756.1902.

5,10,15,20-Tetrakis(4-ethynyl)porphyrin-zinc (II) (**P1-Zn**): To a solution of **P1-TMS-Zn** (1.25 g, 1.6 mmol) in a mixture of CH_2Cl_2 (150 mL) and THF (100 mL) was added TBAF (10.0 mL, 1M in THF). After the mixture was stirred at room temperature for 1 h under Ar, water (200 mL) was added. The solution was concentrated under reduced pressure, filtered, and washed with water. The blue solid was dried under vacuum to give the product in 96% yield (0.705 g). Without further purification, the product was immediately used for subsequent reactions.

5,10,15,20-Tetrakis(4-trimethylsilyl-ethynylphenyl)-porphyrin-zinc (II) (**P2-TMS-Zn**): A solution of *p*-(trimethylsilylethynyl)benzaldehyde (4.04 g, 20 mmol) in propionic acid (150 mL) was stirred in a 250 mL three-neck flask for 1 h at 100 ºC. Pyrrole (1.38 mL, 20 mmol) was added drop wise and the resulting solution was heated under reflux for 3 h while protected from light using aluminum foil. After the solvent was evaporated, the residue was purified through column chromatography (SiO_2; *n*-hexane/$CHCl_3$, from 5:1 to 0:1) to give a purple powder. ^{1}H NMR (400 MHz, $CDCl_3$): δ = -2.881 (s, 2H, pyrrole NH), 0.367 (s, 36H, $SiMe_3$), 7.872&7.852(d, 8H, *m*-H in Ph−C≡C), 8.175&8.154 (d, 8H, *o*-H in Ph−C≡C), 8.853 (s, 8H,

β-pyrrole) ppm. The resulting compound (1.53 g, 1.5 mmol) was dissolved in $CHCl_3$ (100 mL), and saturated methanol of $Zn(OAc)_2 \cdot 2H_2O$ (20 mL) was added. The solution was refluxed for 5 h and then cooled to room temperature. The mixture was added with 100 mL H_2O and evaporated under reduced pressure to remove chloroform and methanol, and the residue was filtered to give a purple powder.

5,10,15,20-Tetrakis(4-ethynylphenyl)-porphyrin-zinc (II) (**P2-Zn**): The porphyrin **P2-TMS-Zn** (1.49 g, 1.5 mmol) was dissolved in THF (100 mL). Then, TBAF (10.0 mL, 1M in THF) was added drop wise to the solution at -78 ºC. The temperature was raised to room temperature slowly and kept overnight. To the reaction mixture, water (100 mL) was added and extracted with $CHCl_3$ (3×150 mL). The organic phase was evaporated to dry to give the product as light purple solid. Yield: 2.0 g, 97%. Without further purification, the product was immediately used for subsequent reactions.

Tetrakis(4-iodophenyl)methane (**I5**): A suspension of tetraphenylmethane (7.52 g, 23.5 mmol), bis(trifluoroacetoxy)iodobenzene (23.5 g, 54.6 mmol), and iodine (12.4g, 49.8 mmol) in carbon tetrachloride (150 mL) was stirred at 50-60°C until the color of iodine disappeared. Carbon tetrachloride was removed by evaporation. The residue was washed with ethanol and acetone and purified by recrystallization in THF to yield 10.9 g (56%) of tetrakis(*p*-iodophenyl)methane as a white crystalline solid. ^{1}H NMR (400 MHz, $CDCl_3$): δ = 6.90 (dd, 8H, *o*-H in Ph), 7.70 (dd, 8H, *m*-H in Ph).

1,3,5,7-Tetrakis(4-iodophenyl)adamantane (**I6**): Iodine (2.36 g, 9.06 mmol) was added to a suspension of tetraphenyladamantane (2.00 g, 4.54 mmol) in chloroform (50 mL) and stirred until the iodine dissolved. Then, (bis(trifluoroacetoxy)iodo)benzene (3.90 g, 9.06 mmol) was added and the suspension was stirred for 24 h at room temperature. The mixture was filtered and the organic layer was washed with $NaHSO_3$ (5%, 50 mL), water (50 mL), brine (50 mL), and dried over $MgSO_4$. The product was crystallized in a chloroform/methanol mixture (9:1) to give colorless crystals of the product (1.90 g, 2.01 mmol, 44%). ^{1}H NMR (400 MHz, $CDCl_3$): δ = 2.05 (s, 12H, CH_2 in adamantane), 7.17 (dd, 8H, *o*-H in Ph), 7.65 (dd, 8H, *m*-H in Ph).

C. Optimization of reaction conditions for the synthesis of por-POFs

1. Solvent

por-POF-7-solv: The polymerization reactions of **P2-Zn** (0.13g, 0.2 mmol) and **I3** (0.12g, 0.2 mmol) in the presence of catalyst $Pd_2(dba)_3/AsPh_3$ were performed in different solvents [solvent:Et_3N = 80 mL:20 mL, solvent = THF, dioxane, NMP, DMF, THF/DMF (1:1)].

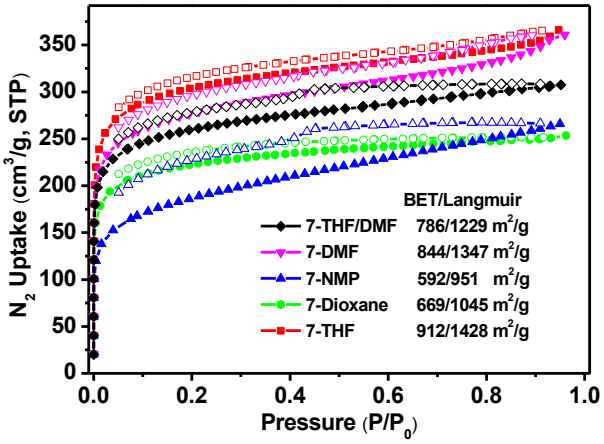

Fig. S1 N_2 sorption isotherms of por-POF-**7**-solv.

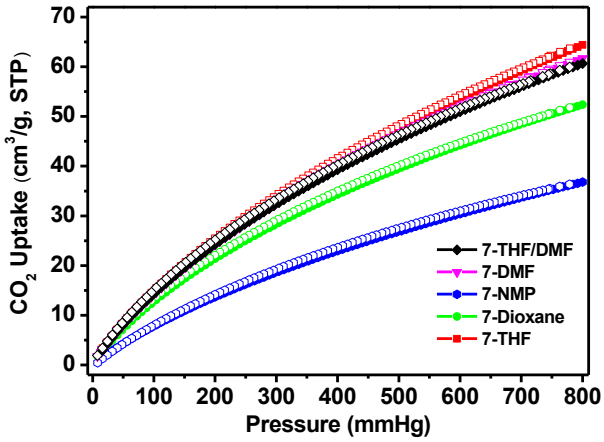

Fig. S2 CO_2 sorption isotherms of por-POF-**7**-solv.

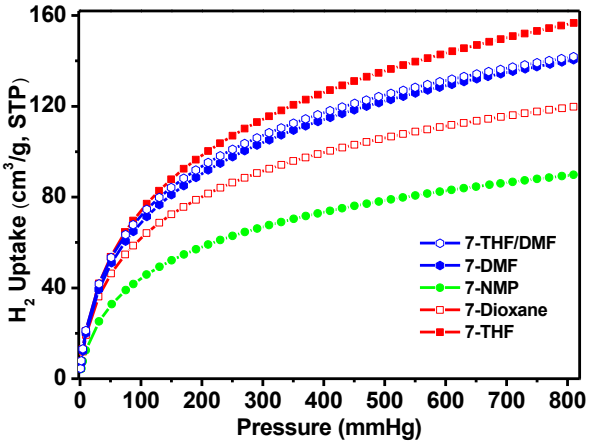

Fig. S3 H_2 sorption isotherms of por-POF-**7**-solv.

2. Reaction temperature

por-POF-7-temp: The polymerization reactions of **P2-Zn** (0.13g, 0.2 mmol) and **I3** (0.12g, 0.2 mmol) in the presence of catalyst $Pd_2(dba)_3/AsPh_3$ were carried out in a solvent mixture of anhydrous THF:Et_3N (80 mL:20 mL) at different temperatures (20 °C, 50 °C, 80 °C, and 100 °C).

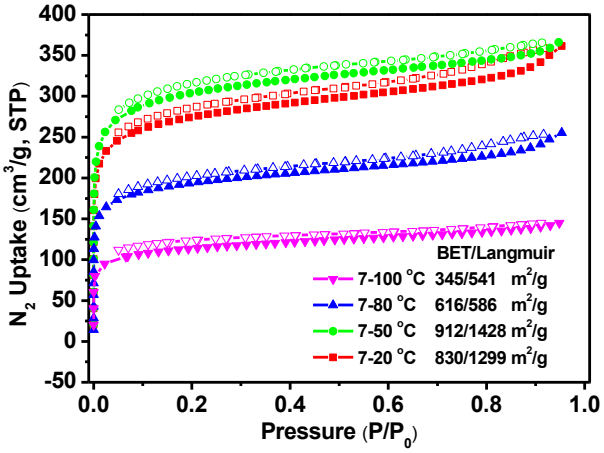

Fig. S4 N_2 sorption isotherms of por-POF-**7**-temp.

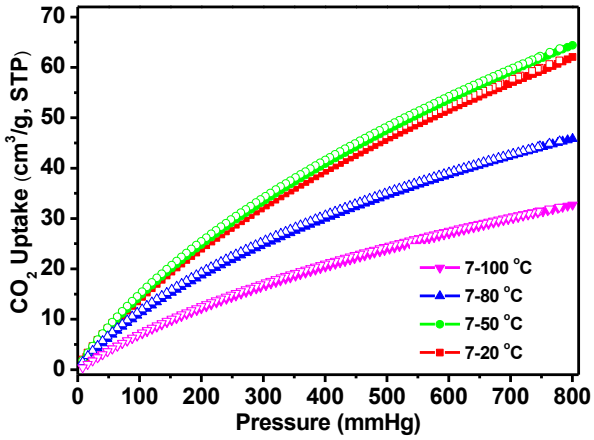

Fig. S5 CO_2 sorption isotherms of por-POF-**7**-temp.

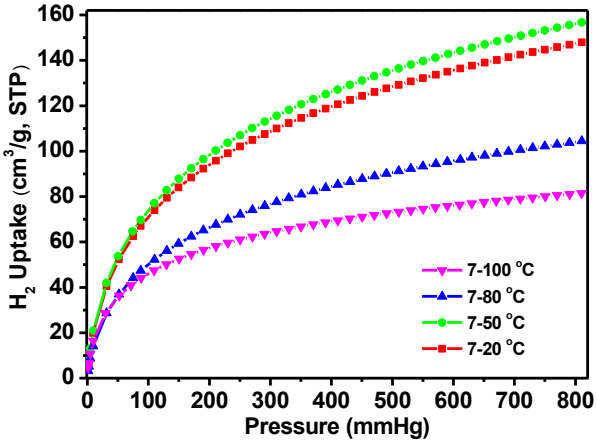

Fig. S6 H_2 sorption isotherms of por-POF-**7**-temp.

3. Monomer concentration

por-POF-7-conc: The polymerization reactions of **P2-Zn** (0.13g, 0.2 mmol) and **I3** (0.12g, 0.2 mmol) in the presence of catalyst $Pd_2(dba)_3/AsPh_3$ were carried out in different amount of solvent THF:Et_3N (4:1, v/v). (20 mM, 40 mM, and 200 mM)

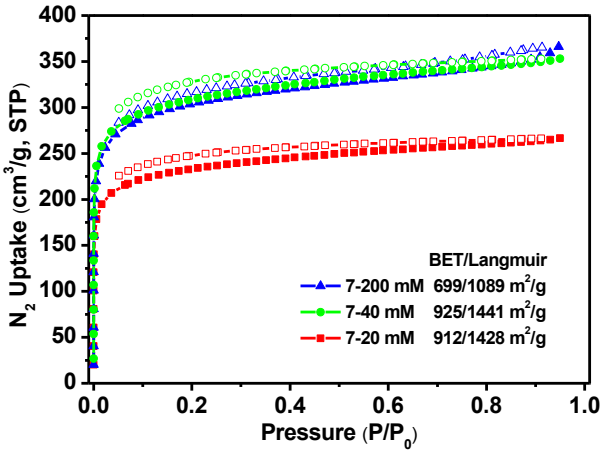

Fig. S7 N_2 sorption isotherms of por-POF-**7**-conc.

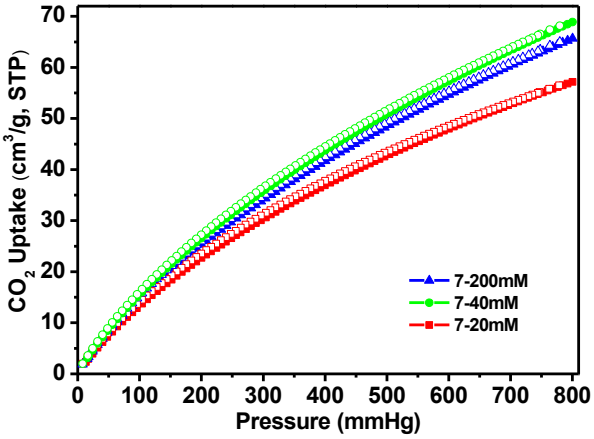

Fig. S8 CO_2 sorption isotherms of por-POF-**7**-conc.

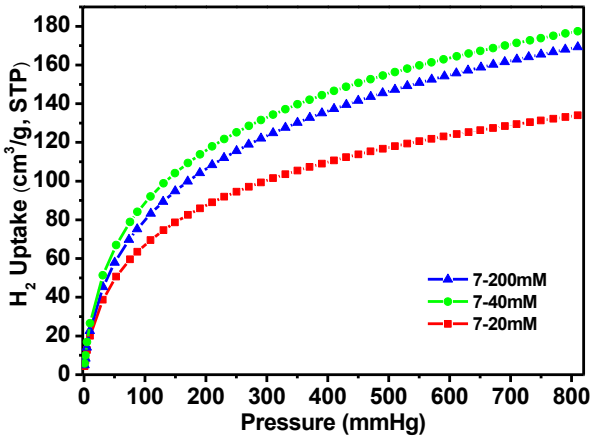

Fig. S9 H_2 sorption isotherms of por-POF-**7**-conc.

4. Ratio of monomer

por-POF-7-ratio: The polymerization reactions of **P2-Zn** and **I3** with different ratio in the presence of catalyst $Pd_2(dba)_3/AsPh_3$ were carried out in solvent of THF:Et_3N (80 mL:20 mL). [ratio = 4:3 (0.2 mmol:0.15 mmol), 3:3 (0.2 mmol:0.2 mmol), 3:4 (0.15 mmol:0.2 mmol), 4:6 (0.2 mmol:0.3 mmol)]

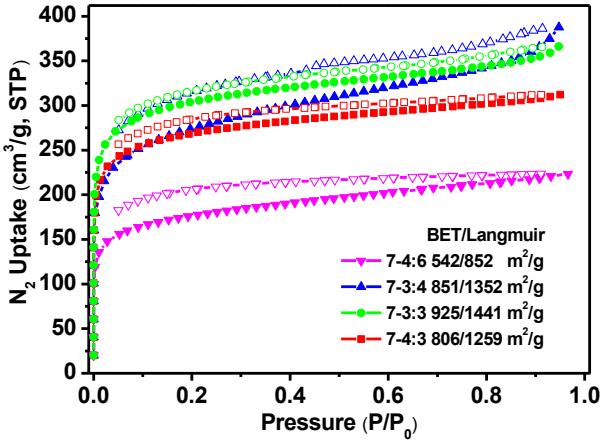

Fig. S10 N_2 sorption isotherms of por-POF-**7**-ratio.

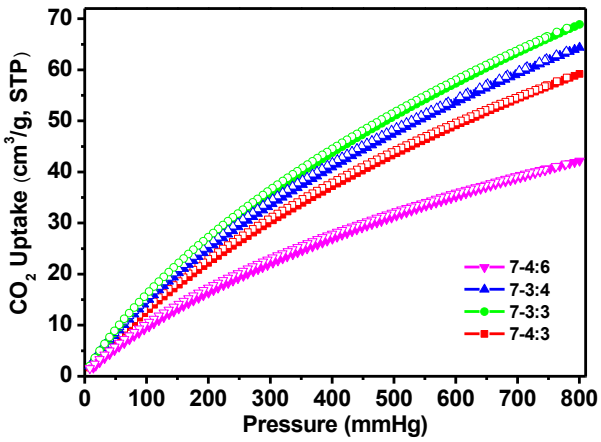

Fig. S11 CO_2 sorption isotherms of por-POF-**7**-ratio.

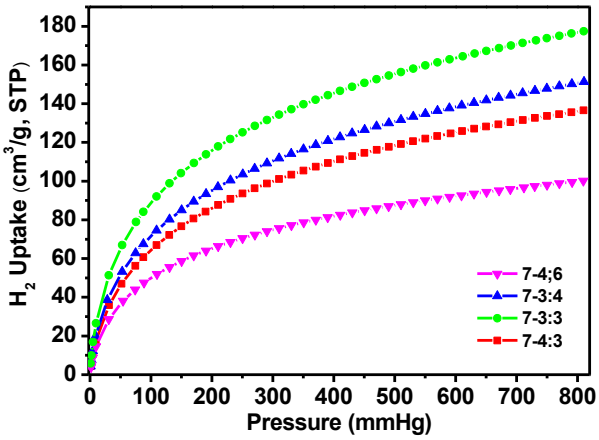

Fig. S12 H_2 sorption isotherms of por-POF-**7**-ratio.

D. Characterization of por-POFs

1. Solid-state CP/MAS ^{13}C NMR spectra

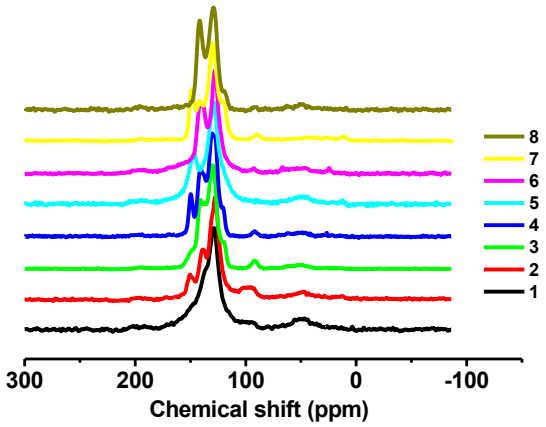

Fig. S13 Solid-state CP/MAS ^{13}C NMR spectra of por-POFs (**1** to **8)**.

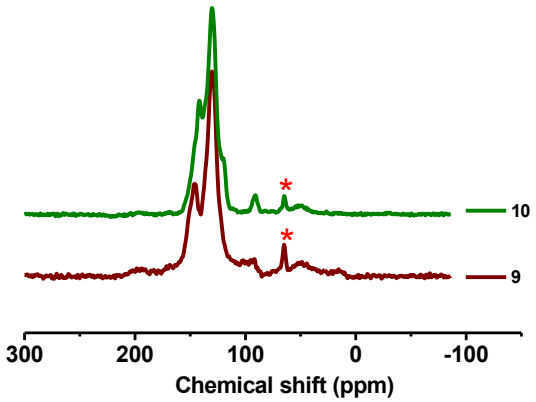

Fig. S14 Solid-state CP/MAS ^{13}C NMR spectra of por-POF-**9,10**. The peak at 64.9 ppm corresponds to the central carbon of the tetraphenylmethane in **I5**.

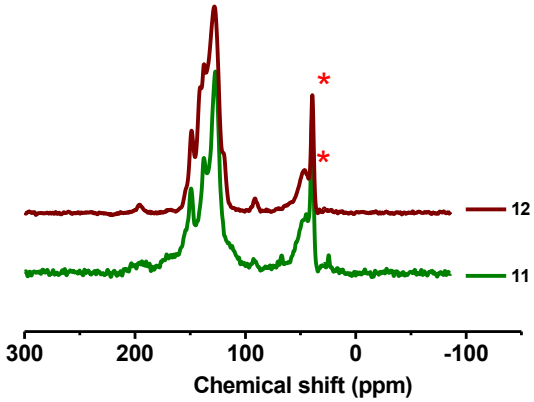

Fig. S15 Solid-state CP/MAS ^{13}C NMR spectra of por-POF-**11,12**. Peaks at 47.0 and 39.4 ppm correspond to the carbon of methylene groups and quaternary carbon from adamantane moiety in **I6**, respectively.

2. Fourier transform infrared (FT-IR) spectra

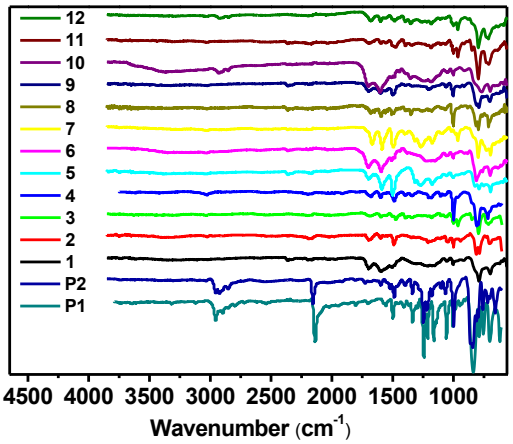

Fig. S16 FT-IR spectra of por-POF-***n*** (***n*** = **1** to **12**).

3. UV-vis spectra

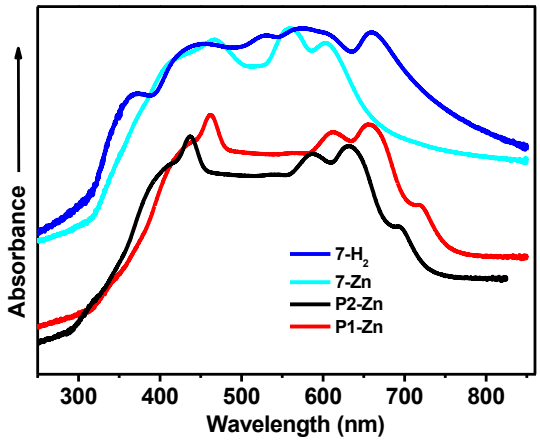

Fig. S17 Solid state UV-vis diffuse reflectance spectra of por-POF-**7**-2H, Zn, P1-Zn, and P2-Zn.

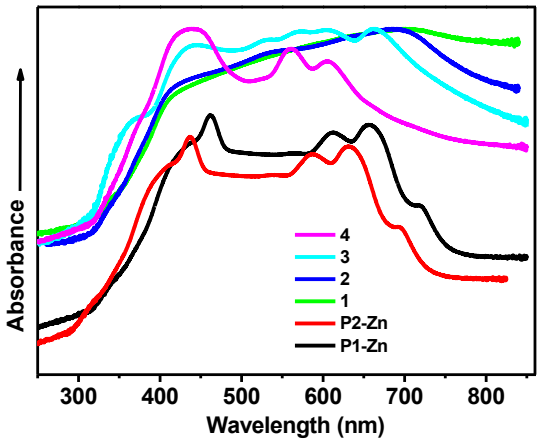

Fig. S18 Solid state UV-vis diffuse reflectance spectra of por-POF-***n*** (***n*** = **1** to **4**).

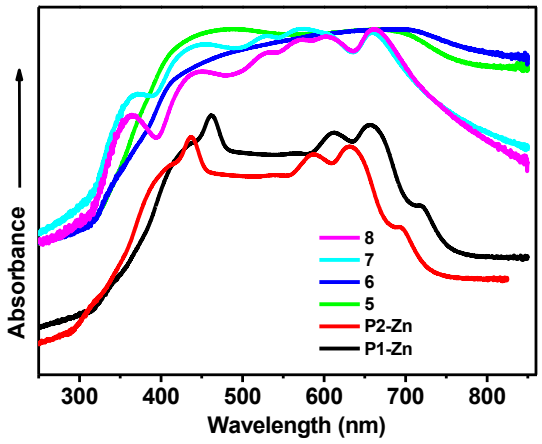

Fig. S19 Solid state UV-vis diffuse reflectance spectra of por-POF-***n*** (***n*** = **5** to **8**).

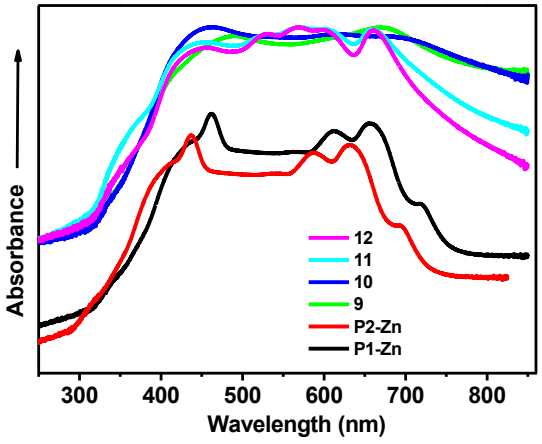

Fig. S20 Solid state UV-vis diffuse reflectance spectra of por-POF-***n*** (***n*** = **9** to **12**).

4. Thermogravimetric analysis

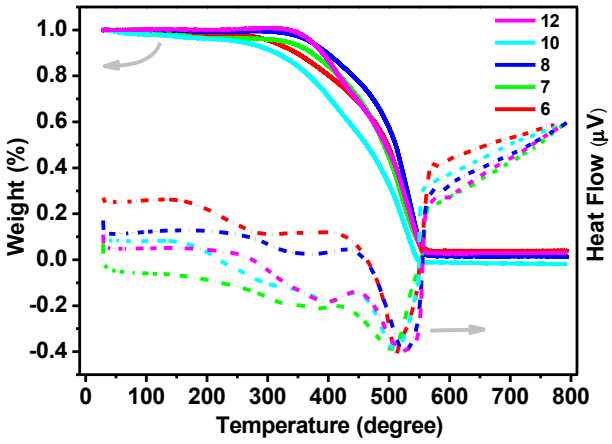

Fig. S21 TGA profiles of por-POFs-***n*** (***n*** = **6**,**7**,**8**,**10**,**12**).

5. N_2, CO_2, and H_2 sorption

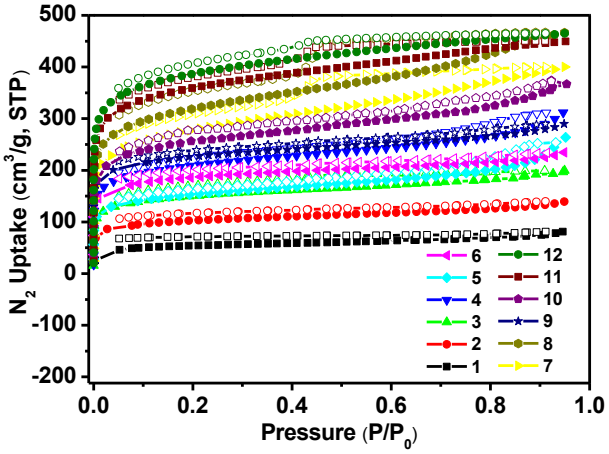

Fig. S22 N_2 sorption isotherms of por-POF-***n*** (***n*** = **1** to **12**).

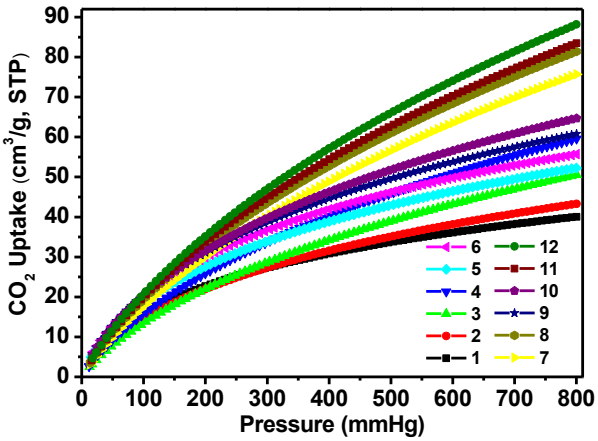

Fig. S23 CO_2 sorption isotherms of por-POF-***n*** (***n*** = **1** to **12**).

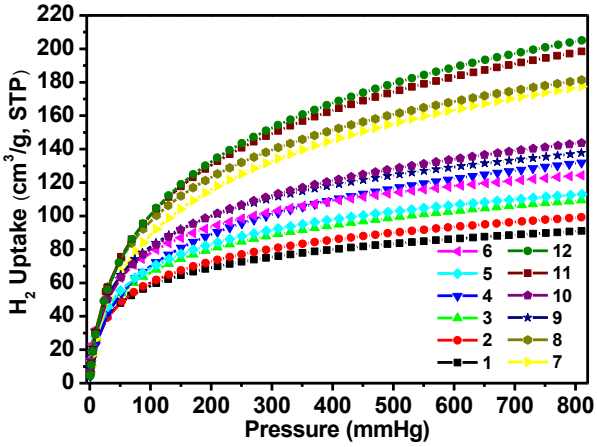

Fig. S24 H_2 sorption isotherms of por-POF-***n*** (***n*** = **1** to **12**).

Table S1 Tabular summary of gas sorption capacities and surface areas of por-POFs

	SA_{BET} ($m^2\ g^{-1}$)	$SA_{Langmuir}$ ($m^2\ g^{-1}$)	SA_{micro} ($m^2\ g^{-1}$)	V_{total} ($cm^3\ g^{-1}$)	V_{micro} ($cm^3\ g^{-1}$)	N_2 77K ($cm^3\ g^{-1}$)	H_2 77K ($cm^3\ g^{-1}$)	CO_2 273K ($cm^3\ g^{-1}$)
por-POF-**1**	189	250	102	0.125	0.051	81	91	40
por-POF-**2**	340	413	197	0.201	0.114	139	99	43
por-POF-**3**	536	647	310	0.296	0.207	199	109	50
por-POF-**4**	745	899	417	0.482	0.228	312	132	60
por-POF-**5**	545	662	294	0.408	0.126	234	113	52
por-POF-**6**	663	802	425	0.363	0.168	264	124	56
por-POF-**7**	987	1195	485	0.619	0.194	400	177	76
por-POF-**8**	1134	1371	596	0.722	0.402	466	181	81
por-POF-**9**	806	982	543	0.448		290	138	61
por-POF-**10**	935	1137	430	0.688	0.172	372	144	65
por-POF-**11**	1279	1546	766	0.695	0.382	450	198	83
por-POF-**12**	1379	1664	846	0.719	0.395	465	205	88

E. Demetallation-remetallation of por-POF-8

1. ICP-MS

Table S2 ICP-MS data of por-POF-**8**-X (X = 2H, FeCl, and Ni)

	^{64}Zn %	^{56}Fe %	^{57}Fe %	^{60}Ni %
por-POF-**8**-2H	0.015	0.000	0.000	0.000
por-POF-**8**-FeCl	0.008	26.41	27.36	0.023
por-POF-**8**-Ni	0.254	0.000	0.000	3.681

2. FT-IR spectra

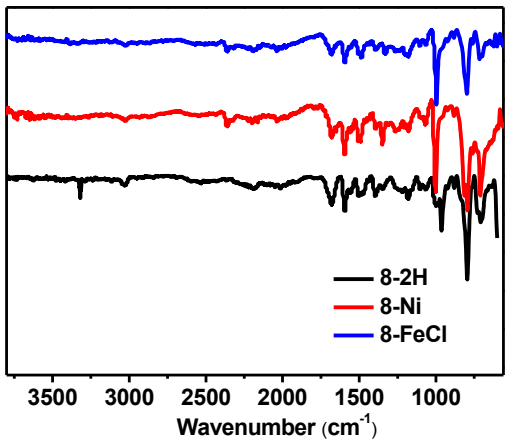

Fig. S25 FT-IR spectra of por-POF-**8**-X (X = 2H, FeCl, and Ni).

3. N_2, CO_2, and H_2 sorption

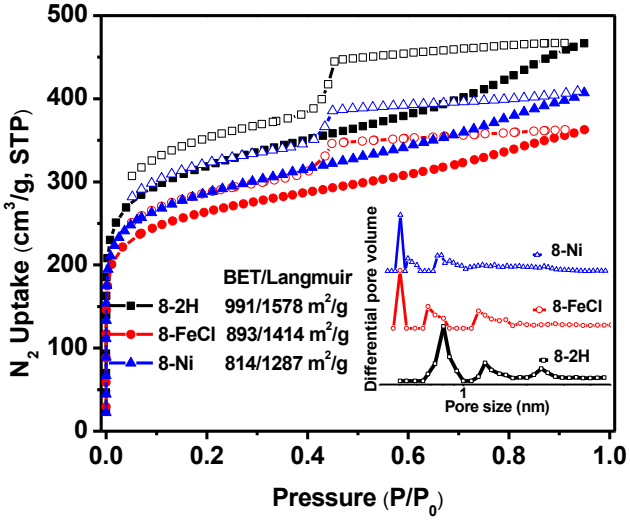

Fig. S26 N_2 sorption isotherms, showing the hysteresis generated from the mesoporosity, of por-POF-**8**-X (X = 2H, FeCl, and Ni). The inset shows the pore size distribution calculated by application of nonlocal density functional theory.

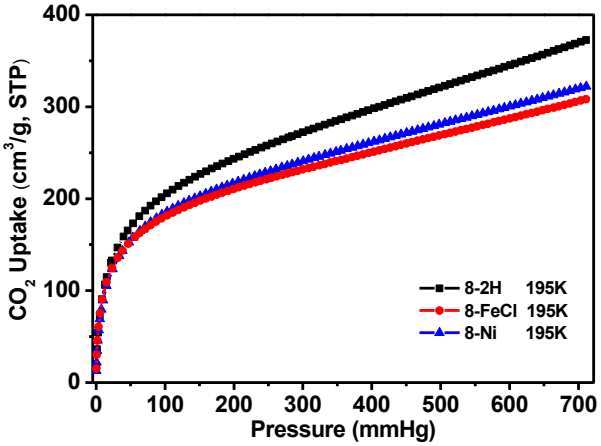

Fig. S27 CO_2 sorption isotherms of por-POF-**8**-X (X = 2H, FeCl, and Ni).

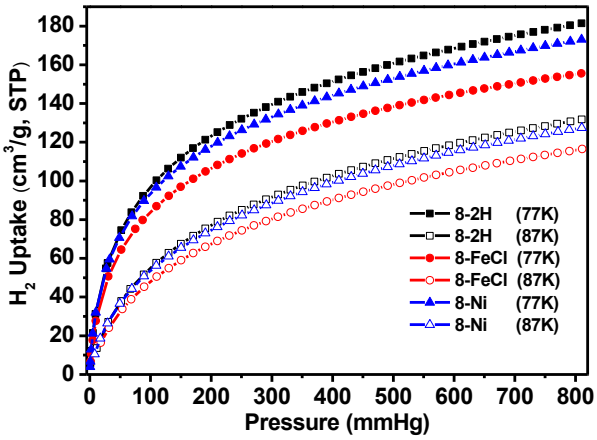

Fig. S28 H_2 sorption isotherms of por-POF-**8**-X (X = 2H, FeCl, and Ni).

4. Isosteric heat of adsorption of por-POF-8-X

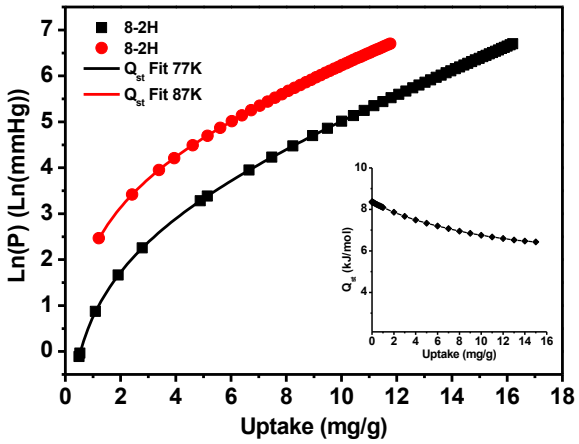

Fig. S29 Isosteric heat of adsorption of por-POF-**8**-2H towards H_2.

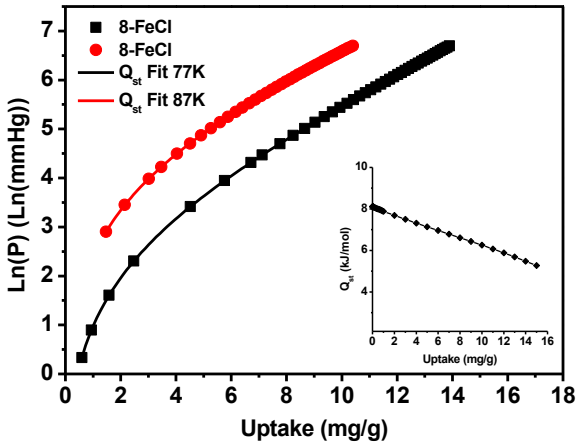

Fig. S30 Isosteric heat of adsorption of por-POF-**8**-FeCl towards H_2.

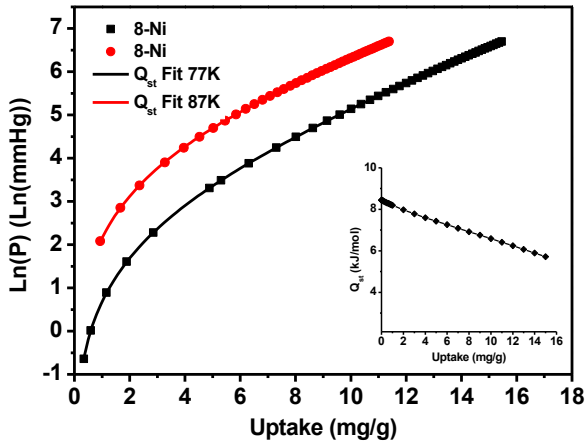

Fig. S31 Isosteric heat of adsorption of por-POF-**8**-Ni towards H_2.

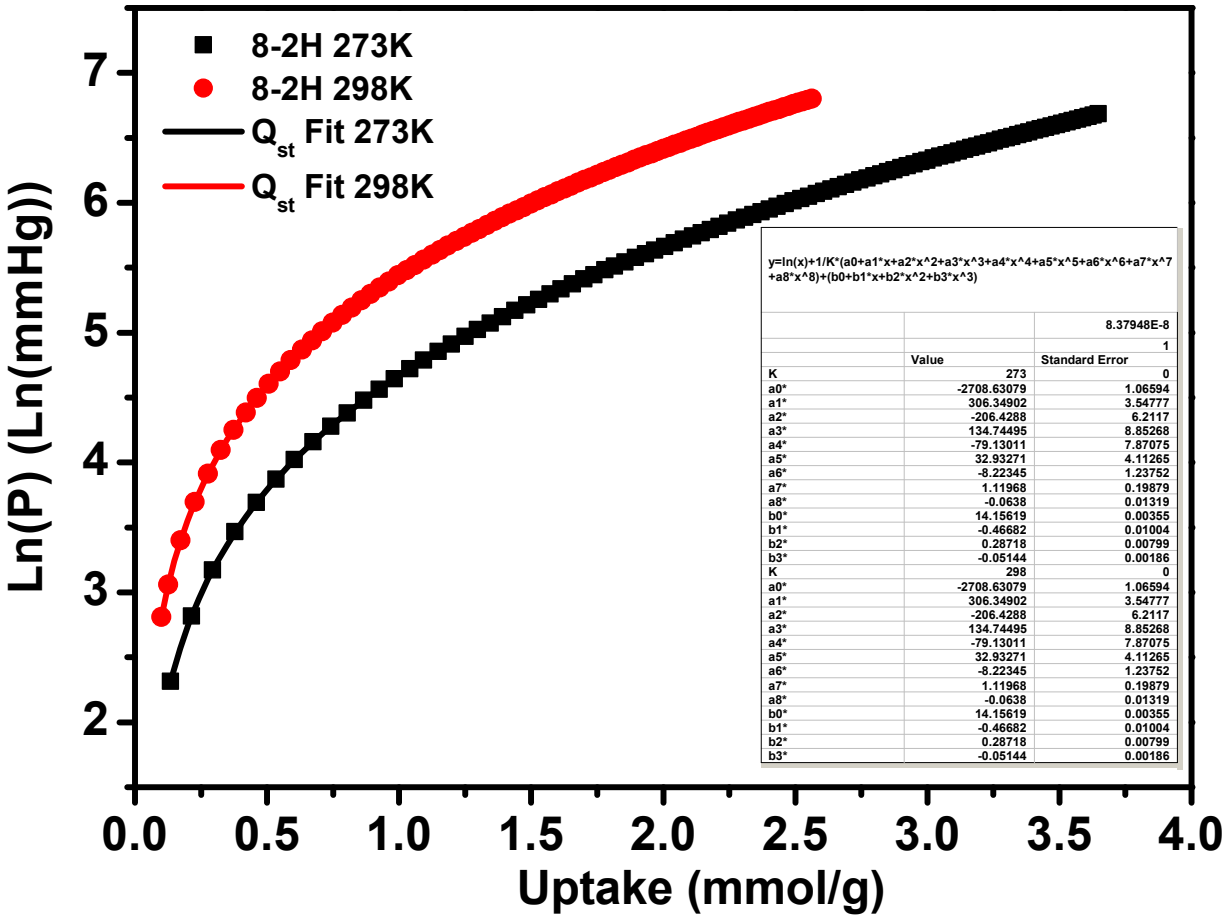

		8.37948E-8
		1
	Value	Standard Error
K	273	0
a0*	-2708.63079	1.06594
a1*	306.34902	3.54777
a2*	-206.4288	6.2117
a3*	134.74495	8.85268
a4*	-79.13011	7.87075
a5*	32.93271	4.11265
a6*	-8.22345	1.23752
a7*	1.11968	0.19879
a8*	-0.0638	0.01319
b0*	14.15619	0.00355
b1*	-0.46682	0.01004
b2*	0.28718	0.00799
b3*	-0.05144	0.00186
K	298	0
a0*	-2708.63079	1.06594
a1*	306.34902	3.54777
a2*	-206.4288	6.2117
a3*	134.74495	8.85268
a4*	-79.13011	7.87075
a5*	32.93271	4.11265
a6*	-8.22345	1.23752
a7*	1.11968	0.19879
a8*	-0.0638	0.01319
b0*	14.15619	0.00355
b1*	-0.46682	0.01004
b2*	0.28718	0.00799
b3*	-0.05144	0.00186

Fig. S32 Isosteric heat of adsorption of por-POF-**8**-2H towards CO_2.

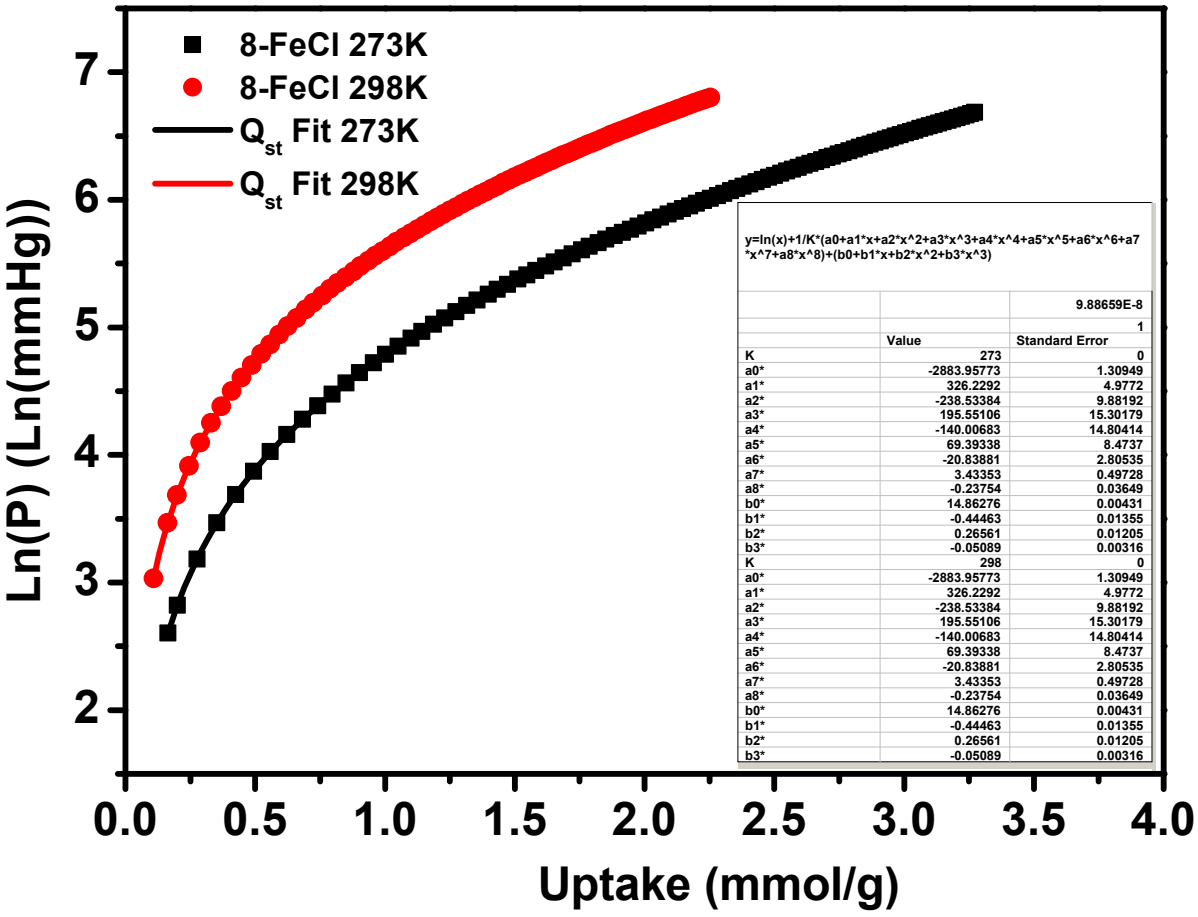

y=ln(x)+1/K*(a0+a1*x+a2*x^2+a3*x^3+a4*x^4+a5*x^5+a6*x^6+a7*x^7+a8*x^8)+(b0+b1*x+b2*x^2+b3*x^3)

		9.88659E-8
		1
	Value	Standard Error
K	273	0
a0*	-2883.95773	1.30949
a1*	326.2292	4.9772
a2*	-238.53384	9.88192
a3*	195.55106	15.30179
a4*	-140.00683	14.80414
a5*	69.39338	8.4737
a6*	-20.83881	2.80535
a7*	3.43353	0.49728
a8*	-0.23754	0.03649
b0*	14.86276	0.00431
b1*	-0.44463	0.01355
b2*	0.26561	0.01205
b3*	-0.05089	0.00316
K	298	0
a0*	-2883.95773	1.30949
a1*	326.2292	4.9772
a2*	-238.53384	9.88192
a3*	195.55106	15.30179
a4*	-140.00683	14.80414
a5*	69.39338	8.4737
a6*	-20.83881	2.80535
a7*	3.43353	0.49728
a8*	-0.23754	0.03649
b0*	14.86276	0.00431
b1*	-0.44463	0.01355
b2*	0.26561	0.01205
b3*	-0.05089	0.00316

Fig. S33 Isosteric heat of adsorption of por-POF-**8**-FeCl towards CO_2.

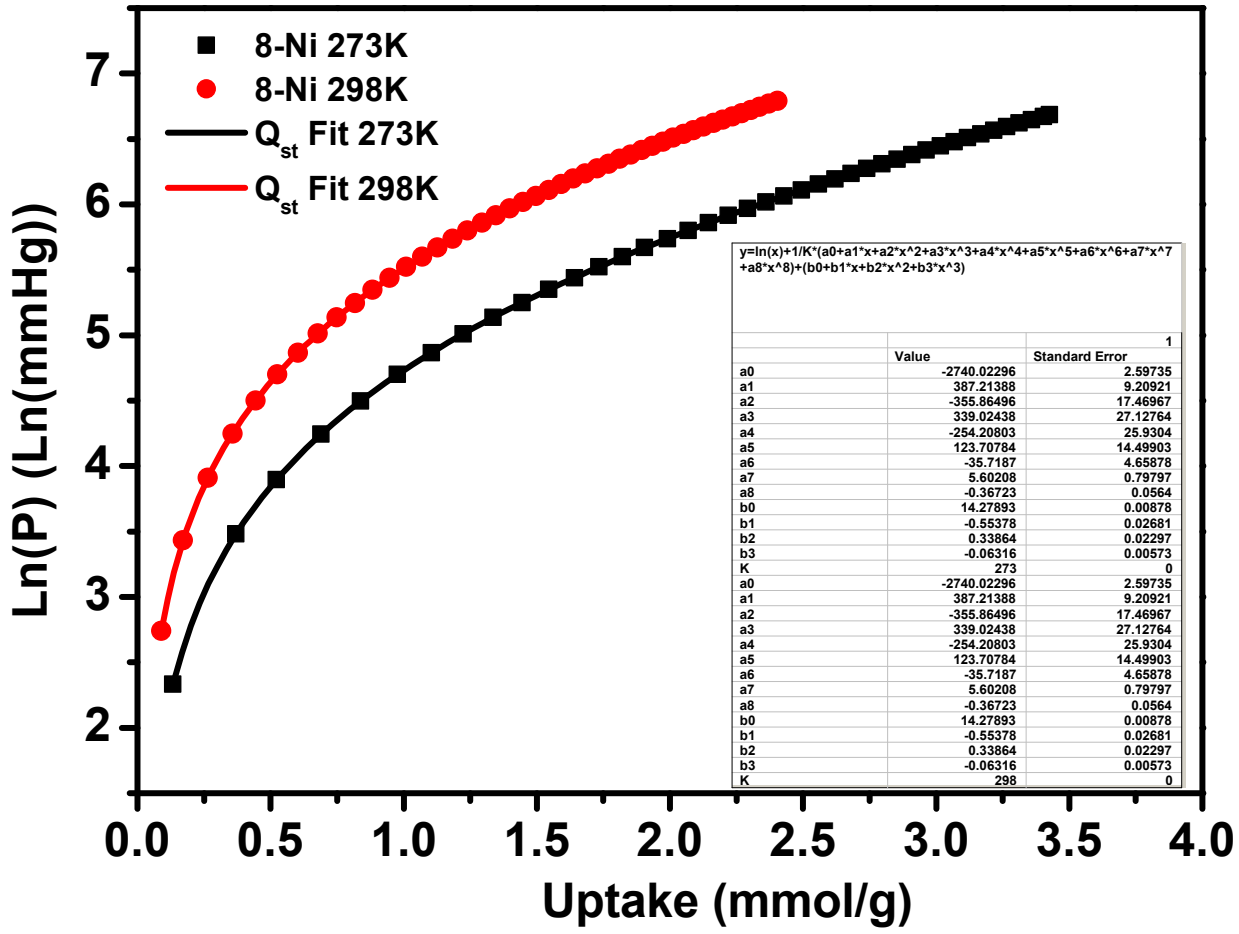

Fig. S34 Isosteric heat of adsorption of por-POF-**8**-Ni towards CO_2.

Table S3 A summary of gas sorption capacities and surface areas of por-POF-**8**-X (X = 2H, FeCl, and Ni)

	$SA_{BET}/S_{Langmuir}$ ($m^2\ g^{-1}$)	H_2 ($cm^3\ g^{-1}$)		CO_2 ($cm^3\ g^{-1}$)		
		77 K	87 K	195 K	273 K	298 K
8-2H	991/1578	176	132	372	82	57
8-FeCl	814/1287	151	116	308	73	50
8-Ni	893/1414	168	127	322	77	54

F. Computational analysis of binding energies

Geometric structure optimization and frequency calculations are performed using a density-functional theory (DFT) method implemented in G09 package. The functional ωB97XD is chosen includes dispersion correction. To reduce computing cost, we only focus on smaller systems to evaluate the H_2 and CO_2 adsorption energies on different porphyrin macrocycle. The optimized geometries of four H_2 molecules adsorbed to the same side surface of free base porphyrin (por-2H) or that of metallated porphyrins (por-FeCl and por-Ni) are shown in Figure S35 while the optimized geometries of CO_2 adsorbed to a side surface of por-2H, pro-FeCl, or por-Ni are shown in Figure S36. As shown in Figure S35, H_2 cannot be adsorbed vertically above the center of porphyrin macrocycle. We thus only obtain the geometries of four H_2 co-adsorbed on the same side surface of porphyrin macrocycle. On the other hand, as displayed in Figure S36, one of oxygen atoms in CO_2 is located vertically above the center of porphyrin macrocycle. Therefore, only one CO_2 can be adsorbed on a side surface of porphyrin macrocycle.

To obtain more reliable interaction energies (adsorption energies, E_{ad}), the basis set superposition error (BSSE) corrections are considered [E_{ad} is computed according to the formula $E_{ad} = E_{corrected} - (E(1) + E(2) + ... E(j) ... + E(n))$, where $E_{corrected} = E_{complex} + E_{BSSE}$, and $E(j)$ means the energy associated with monomer centered basis set (MCBS) calculation for fragment j]. The computed adsorption energies are listed in Table S1. The order of H_2 binding is por-2H > por-Ni > por-FeCl, but actually the difference in H_2 binding among the three macrocycles is quite small. The average adsorption energies per H_2 computed at the ωB97XD/6-311G(d,p) level are -6.08, -5.55 and -4.90 kJ/mol for por-2H, por-Ni, and por-FeCl, respectively. Similarly, the computed CO_2 adsorption energies are almost same for por-2H and por-FeCl. Therefore we can conclude that there is no significant change in the adsorption energies of H_2 and CO_2 adsorption after Ni and $FeCl_3$ coordinate to the center of porphyrin.

Table S1 Adsorption energies of H_2 and CO_2 adsorbed to porphyrin and its metal complexes (see Figure S35 and S36 below)

	E_{ad}, KJ/mol ωB97XD/6-311G(d,p)
por-2H - 4H_2	-24.30
por-Ni - 4H_2	-22.21
por-FeCl - 4H_2	-19.59
por-2H - CO_2	-14.38
por-Ni - CO_2	-13.32
por-FeCl - CO_2	-14.49

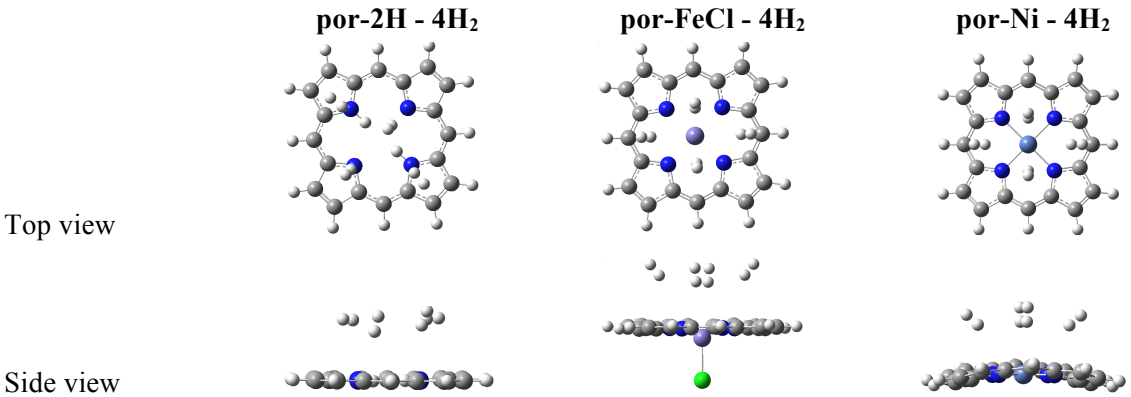

Fig. S35 Optimized structures by ωB97XD/6-311G(d,p) when four H_2 adsorbed on the same side of porphyrin and its metal complexes (grey, carbon; white, hydrogen; blue, nitrogen; green, chlorine; purple, iron; light blue, nickel).

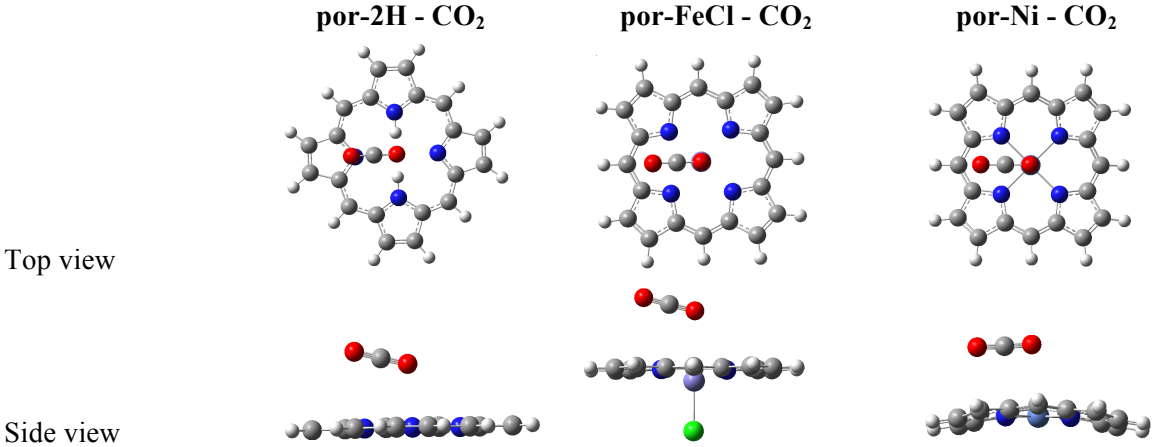

Fig. S36 Optimized structures by ωB97XD/6-311G(d,p) when one CO_2 adsorbed on the same side of porphyrin and its metal complexes (grey, carbon; white, hydrogen; red, oxygen; blue, nitrogen; green, chlorine; purple, iron; light blue, nickel).